Photothermal Circular Dichroism Induced by Plasmon Resonances in Chiral Metamaterial Absorbers and Bolometers

Xiang-Tian Kong,[†,‡,a] Larousse Khosravi Khorashad,[‡,a] Zhiming Wang,[*,†]

Alexander O. Govorov[*,‡]

[†]Institute of Fundamental and Frontier Sciences, University of Electronic Science and Technology of China, Chengdu 610054, China

[‡]Department of Physics and Astronomy, Ohio University, Athens, Ohio 45701, United States

[a] Equal contributors

* E-mails: jmwahng@gmail.com; govorov@ohio.edu

ABSTRACT

Chiral photochemistry remains a challenge because of the very small asymmetry in the chiro-optical absorption of molecular species. However, we think that the rapidly developing fields of plasmonic chirality and plasmon-induced circular dichroism demonstrate very strong chiro-optical effects and have the potential to facilitate the development of chiral photochemistry and other related applications such as chiral separation and sensing. In this study, we propose a new type of chiral spectroscopy – photothermal circular dichroism. It is already known that the planar plasmonic superabsorbers can be designed to exhibit giant circular dichroism signals in the reflection. Therefore, upon illumination with chiral light, such planar metastructures should be able to generate a strong asymmetry in their local temperatures. Indeed, we demonstrate this chiral photothermal effect using a chiral plasmonic absorber. Calculated temperature maps show very strong photothermal circular dichroism. One of the structures computed in this paper could serve as a chiral bolometer sensitive to circularly polarized light. Overall, this chiro-optical effect in plasmonic metamaterials is much greater than the equivalent effect in any chiral molecular system or plasmonic bio-assembly. Potential applications of this effect are in polarization-sensitive surface photochemistry and chiral bolometers.

KEYWORDS: Chiral plasmonics, Circular dichroism, Photothermal effect, Heat generation

Since life is chiral, the topic of manipulation and separation of chiral species will always remain relevant for research and technology.[1] Chiral light is a very handy tool, therefore, for technologies related to the life sciences. Light beams with opposite handedness interact differently with chiral matter and cause different dissipation and reaction. Circular dichroism (CD) spectroscopy is one of the most powerful methods to probe the chirality of biomolecules.[2] However, it is a challenging task to make chiral light-matter interactions sufficiently strong to be suitable for practical applications. Recent developments in this direction include: (1) Observations of strong CD signals in plasmonic bio-assemblies;[3,4,5] (2) fabrication of metal and semiconductor nanocrystals with chiral shapes;[6,7,8,9,10] (3) reports on chiral interactions between quantum dots and biomolecules;[11] (4) plasmon-induced CD in biomolecular-plasmonic complexes;[12,13,14,15,16,17] (5) investigation of chiral planar nanostructures with and without biomolecular coatings;[18,19,20,21,22,23] (6) realization of a chiral photodetector based on metamaterials;[24] (7) measurement of asymmetric optical forces between a chiral plasmonic tip and a substrate.[25]

Here we describe a new type of chiro-optical effect that involves a combination of plasmonics and thermal physics. Photothermal circular dichroism (photothermal-CD), described in this paper, is an effect of strong asymmetry in the photogenerated temperature in a chiral metastructure. It is well established that plasmonic nanocrystals are excellent photoheaters.[26,27] This property enables many photothermal applications of plasmonic nanoparticles in the biomedical field[28,29,30,31,32,33] and in physical chemistry.[34,35,36,37] The geometry of a plasmonic heater is an important factor to achieve the desired temperature distributions.[38,39,40] Simultaneously, plasmonic nanostructures and metamaterials enable interesting possibilities to manipulate light.[41] One well recognized effect in plasmonic planar metamaterials is that of a

strong optical absorption in an optically-thin system.[42,43,44,45] Such nearly-perfect absorbers consist of a top layer of plasmonic resonators and a back reflector.[43,44,45,46] The spacing between two layers in a superabsorber can be made much smaller than the wavelength of incident light. A superabsorber nanostructure may have an absorption coefficient close to unity at a few wavelengths. Correspondingly, chiral absorbers with asymmetric top-layer plasmonic resonators can demonstrate very strong CD signals.[24] Chiral elements in metamaterials can be asymmetric nanowires,[24] S- or L-shaped nanocrystals,[19,22] as well as having many other shapes.[18,20] Here we use the idea of a perfect absorber[42] and combine it with the photothermal effect in a plasmonic nanostructure.[27,38] As a physical system to demonstrate the photothermal CD effect, we choose the geometry of the perfect absorber with Γ-shaped nanocrystals. Our study shows that large optical CD is translated to strong chiral photothermal signals. The photothermal-CD effect mostly scales with the optical CD signal. Our numerical simulations yield local maps for the photothermal-CD effect in the chiral metastructure absorber.

CD and *g*-factor are the commonly-used observable parameters characterizing a chiral nanostructure:

$$CD = A_{\mathrm{LCP}} - A_{\mathrm{RCP}}, \quad g_{\mathrm{CD}} = \frac{A_{\mathrm{LCP}} - A_{\mathrm{RCP}}}{\left[A_{\mathrm{LCP}} + A_{\mathrm{RCP}}\right]/2}, \tag{1}$$

where A_{LCP} and A_{RCP} are the absorptances of the chiral nanostructure illuminated by the left and right circularly polarized beams, respectively. In a similar fashion, we define the parameters for the photothermal-CD effect. Photothermal CD is defined as a difference of photoinduced temperatures,

$$CD_T(\mathbf{r}) = \delta T(\mathbf{r}) = \Delta T_{\mathrm{LCP}}(\mathbf{r}) - \Delta T_{\mathrm{RCP}}(\mathbf{r}), \tag{2}$$

where $\Delta T_{\mathrm{LCP}}(\mathbf{r})$ and $\Delta T_{\mathrm{RCP}}(\mathbf{r})$ are the local temperature increases created by the left and right

circularly polarized beams, respectively. Correspondingly, a chiral *g*-factor for the photothermal CD effect is defined as

$$g_T = \frac{\Delta T_{\mathrm{LCP}}(\mathbf{r}) - \Delta T_{\mathrm{RCP}}(\mathbf{r})}{\left[\Delta T_{\mathrm{LCP}}(\mathbf{r}) + \Delta T_{\mathrm{RCP}}(\mathbf{r})\right]/2}. \tag{3}$$

The above photothermal chiral properties are local and depend on the position. Overall, since temperature is induced via the optical absorption process, the optical and thermal CD effects should produce similar *g*-factors, i.e., $g_T \sim g_{CD}$. This property can be illustrated using the simplest case of a small spherical nanocrystal. The temperature increase on the surface of a single plasmonic nanoparticle of small size under CW illumination is given by[38,47]

$$\Delta T_{\mathrm{surface}} = \frac{Q_{\mathrm{tot}}}{4\pi k_t}\frac{1}{R_{\mathrm{NP}}} \tag{4}$$

where Q_{tot} is the total rate of heat dissipation, R_{NP} is the nanoparticle radius and k_t is the thermal conductivity of a surrounding medium; the heat conductivity of the metal can be considered as infinite. From Eq. 4, we see that the local increase in temperature is directly proportional to the absorption rate and, therefore, we can assume for an arbitrary chiral system the correspondence between the *g*-factors, $g_T \sim g_{CD}$. We will see this property in our computational results obtained for complex chiral metastructures.

However, one can also see a qualitative difference between the optical and thermal *g*-factors: the factor g_{CD} describes a whole nanostructure, whereas the factor $g_T(\mathbf{r})$ is local and depends on the position where the photoinduced temperature is measured. For applications related to surface photochemistry, the average temperature on the surface can be a useful parameter. A related photochemical experiment with photoinduced melting of molecules adsorbed on a metal nanostructure was reported recently in Ref. 48. Another application lies in designing

metastructure bolometers.[45] In this case, one should compute a temperature increase averaged over a slab of a temperature-sensitive crystal located near the absorbing metastructure. In this scheme, the electric resistance of the temperature-sensitive slab (doped silicon layer embedded inside silicon nitride) is used to determine the local temperature. In turn, the measured local temperature in the bolometric slab tells us about the absorption rate and intensity of an incident circularly polarized beam.

1. Model and photothermal formalism.

Figure 1a shows the geometry of our Γ-shaped metamaterial. It consists of the asymmetric top-layer nanostructures made of silver and the back reflector made of gold. Such combination of plasmonic metals (silver and gold) was used recently in Ref. 49. We note that the back reflector can also be made of silver and the final results for the photothermal effects in such a case will remain overall similar to the results reported in this paper. The spacing between the plasmonic layers is made of polymer with a low thermal conductivity. In this case, the photoinduced temperature under the pulse excitation becomes strongly localized in the top plasmonic layer. The medium above the metastructure was chosen to be water or air. In the main design used in this paper, the substrate is made of glass, which has a low thermal conductivity. In the case of the bolometric structure, the substrate material was taken to be silicon nitride, like in Ref. 45.

Our plasmonic absorber is under pulsed optical excitation (Figure 1a) and the central function to be calculated is the local increase of temperature, $\Delta T(\mathbf{r},t) = T(\mathbf{r},t) - T_0$, where T_0 is the ambient temperature and $\mathbf{r}$ and t are the coordinate and time, respectively. The heat transfer equation for our photoexcited system reads

$$\rho(\mathbf{r})\, c(\mathbf{r}) \frac{\partial \Delta T(\mathbf{r},t)}{\partial t} = \vec{\nabla}\left[k(\mathbf{r}) \vec{\nabla} \Delta T(\mathbf{r},t) \right] + Q(\mathbf{r},t) \tag{5}$$

In this equation, $\rho(\mathbf{r}), c(\mathbf{r})$ and $k(\mathbf{r})$ are the mass density, specific heat and thermal conductivity, respectively. The local heat intensity $Q(\mathbf{r},t)$ comes from the light dissipation in the plasmonic components of the system:

$$Q(\mathbf{r},t) = \left\langle \mathbf{j}(\mathbf{r},t) \cdot \mathbf{E}(\mathbf{r},t) \right\rangle_t = \frac{\omega}{8\pi} \left| \mathbf{E}_\omega(\mathbf{r}) \right|^2 \cdot \mathrm{Im}\, \varepsilon(\mathbf{r}) \cdot Pulse(t) \tag{6}$$

where $\mathbf{j}(\mathbf{r},t)$ is the electric current density, $\mathbf{E}(\mathbf{r},t)$ is the electric field inside the system and $\varepsilon(\mathbf{r})$ is the local dielectric constant of the system. The function $\mathbf{E}_\omega(\mathbf{r})$ is the complex field amplitude. The excitation is via an optical pulse with the duration of 8 ns. Correspondingly, the pulse function has the form: $Pulse(t) = 1$ for $0 < t < 8ns$ and $Pulse(t) = 0$ otherwise. Since the plasmonic reaction time is very short, this local field in Eq. 6 can be calculated as a reaction to the external monochromatic excitation. The incident beam is normal to the metamaterial and has the standard form: $\mathbf{E}_0(\mathbf{r},t) = \mathbf{E}_0 \cdot \mathrm{Re}\left[e^{-i\omega t + i\mathbf{k}\cdot\mathbf{r}} \right]$, where $\mathbf{E}_0$ is the amplitude of the incident field. The incident flux and the field amplitude of light are related through $I_0 = c_0 \left| \mathbf{E}_0 \right|^2 \sqrt{\varepsilon_0} / 8\pi$, where c_0 is the speed of light in vacuum. The optical and thermal parameters of the components of our system are summarized in Table 1. The dielectric constants of the plasmonic metals (Au and Ag) were taken from Ref. 50. The electromagnetic fields and local temperature distributions were computed for the models of interest using the COMSOL software package.

Table 1. Thermal and optical parameters of the materials used in our metastructures.

	Thermal conductivity, k [$W \cdot m^{-1} \cdot K^{-1}$]	Mass density, ρ [$g \cdot cm^{-3}$]	Specific heat capacity, c [$J \cdot g^{-1} \cdot K^{-1}$]	Heat diffusivity, $K_{diff} = k \cdot \rho^{-1} \cdot c^{-1}$ [$m^2 \cdot s^{-1}$]	Dielectric constant, ε_0
Water	0.6	1	4.181	1.43×10^{-7}	1.8
Glass (SiO_2)	1.4	2.65	0.840	6.29×10^{-7}	2.13
Polymer (PMMA)	0.2	1.18	1.27	1.33×10^{-7}	2.25
Ag	407	10.50	0.233	1.66×10^{-4}	ref 50
Au	318	19.32	0.129	1.27×10^{-4}	ref 50
Air	0.024	1.2×10^{-3}	1.012	1.98×10^{-5}	1
Si_3N_4	30	3.25	1	9.23×10^{-6}	4.08

2. **Results for the photothermal CD effect.**

Computational results in Figures 1 and 2 provide us with an overview of the optothermal effects in the metastructure. As expected, the electromagnetic fields become localized in the gap between the plasmonic Γ-nanocrystal and the back contact (Figure 1b). Simultaneously, optical absorption and heat generation mainly take place in the metal nanostructures as one can see from the maps of the photoinduced temperature (Figure 1c). The system exhibits two main plasmonic resonances in the near-infrared spectral range (Figure 2a,b). These plasmonic resonances correspond to the two coupled modes of the two arms of the Γ-nanocrystal. Figure 2e shows the surface charge distributions of the system at the two plasmonic absorption peaks with linearly polarized light. Since the geometry of the nanostructure is complex, the character of optical excitation in the system is multipolar. Due to the strong plasmonic resonances and the geometrical chirality of the Γ-shape, the system shows a strong CD effect and large *g*-factors near the plasmonic resonances (Figure 2c,d).

The main result of this study is a strong photothermal CD effect (Figures 3 and 4). Such a strong asymmetry of generation of phototemperature is a peculiar property of a plasmonic metamaterials. So far, only specially-designed asymmetric metamaterials were able to show *g*-

factors close to unity for the visible and near-infrared spectral intervals. Correspondingly, such structures become ideal for demonstration of the strong photothermal CD effect. Figure 3 shows spatial maps of the photoinduced temperature and the related photothermal CD. The maps are shown at different vertical positions; the positions $z = 0$ and 40 nm correspond to the bottom and top surfaces of the Γ-nanostructure, respectively (Figure 1a). We observe strong local photothermal CD in the vicinity of the top plasmonic layer where the major process of light dissipation takes place. The local photothermal effect, of course, decays as we move away from the absorber in the vertical (+z) and lateral directions. The photoinduced temperature increase is nearly uniform inside the Γ-nanostructure at $t = 8$ ns because of the large heat diffusivity of the metal. Figure 4 presents the spectra of the photothermal effects in our chiral system at one selected position, point P_1. Supporting Information has data for two more spatial positions, P_2 and P_3. From Figure 4, we see that the photothermal g-factor is ~ 0.5 and is similar in magnitude to the optical g-factor in Figure 2. This agrees with our qualitative arguments given above in the introduction section.

Finally, we look at the spatial-temporal distributions of temperature. Figure 5a,b describes the metamaterial device for surface photochemistry, whereas Figure 5c is related to the case of a chiral bolometer. During and after the pulse, the temperate distribution within the metal nanostructure is nearly flat (Figure 5a) since the thermal conductivity of the metal is high. With time, heat generated in the metastructure absorber diffuses into the surrounding media and, accordingly, the photoinduced temperature decays (Figure 5b, on the left). During the pulse, the temperature distribution is strongly peaked at the top nanocrystal and, as time goes on, we observe the typical effect of diffusive spreading of the local heat (Figure 5b, on the right). In the structure for photochemistry, both bulk media (water and glass) have similar heat conductivities

and, therefore, the photoinduced heat diffuses in both media. In the case of the bolometric structure, heat mostly diffuses into the solid substrate since it has a much higher thermal conductivity as compared to air. However, the temperature of air near the nanostructure rapidly increases during the optical pulse since air has a high thermal diffusivity and a low heat capacity. Since the density of air is so low, the total amount of heat in air remains small despite the large temperature increase in the air region. In the bolometric structure exposed to air, most of the photoinduced heat diffuses into the device and the temperature increase in the silicon nitride causes a change in the electrical resistance of the substrate.[45]

3. Discussion

It is interesting to compare the magnitudes of photothermal CD in our metastructures and in the other chiral systems, such as biomolecules and plasmonic nanocrystal assemblies. First, we note here that the *g*-factors vary in the following limits: $0 < g_{CD} < 2$ and $0 < g_T < 2$. Second, as it was mentioned in the introduction, the photothermal and optical *g*-factors should be of the same order of magnitude, i.e., $g_{CD} \sim g_T$. Indeed, we see this correspondence in Figures 2 and 4. In chiral biomolecules (proteins, DNAs, etc), the typical asymmetry factor is $g_{CD} \sim 10^{-3}$.[2] Plasmonic nanocrystal assemblies with chiral geometries can show much larger *g*-factors, ~ $2 \cdot 10^{-2}$.[4,51] In the metastructure absorbers with the two-layer geometry, the *g*-factor can be as high as 1.1.[24] So high *g*-factor for the perfect absorber realized in Ref. 24 comes from its design in which the metal nanostructures (chiral nanowires) are embedded into a medium with a high refractive index (silicon). In the systems studied in this paper, we used the media with smaller refractive indices (water and polymer) and, therefore, the magnitudes of absorption coefficients

and the maximum asymmetry parameters were somewhat smaller, $g_{CD} \sim g_T \sim 0.5$. Yet, these *g*-factors are much higher than those in biomolecules and plasmonic bio-assemblies. The choice of the materials in our models was dictated by potential applications, which are in surface photochemistry and in chiral photodetectors and bolometers.

Finally, we comment on potential applications of the proposed nanostructures. In a chiral device for photochemistry, rates of thermally-activated reactions on the surface of an absorber will depend on the handedness of incident light beam. A chiral bolometer proposed here can be used to measure the degree of circular polarization of the incident light. For this, the device should have two metamaterial absorber panels with the different chiralities and both panels should be illuminated with the same incident beam. Then, the difference in the bolometric response of the two absorbers will tell us about the presence of circular polarization in the incident beam.

4. Conclusions

In this computational study, we have described the effect of photothermal plasmonic CD. This effect is unique for plasmonic metamaterial absorbers since it requires two conditions: (1) Efficient absorption of light resulting in strong and localized heating [52] and (2) a strong CD effect. On the one hand, plasmonic nanocrystals are excellent absorbers and heaters. On the other hand, chiral plasmonic metamaterials can generate a giant CD effect with *g*-factors close to unity. The combination of the above two factors can enable a strong photothermal CD effect. Indeed, the chiral plasmonic absorber designed in this study has shown very large photothermal *g*-factors, ~

0.6. Chiral metamaterial heaters can be potentially used for surface photochemistry and to create bolometers sensitive to the circular polarization of incident light.

Supporting Information

Details regarding the photothermal properties of chiral metamaterial absorbers. The Supporting Information is available free of charge on the ACS Publications website

ORCID

Xiang-Tian Kong: 0000-0002-8554-0369

Alexander O. Govorov: 0000-0003-1316-6758

Acknowledgements

X.-T.K. was supported by China Postdoctoral Science Foundation (2015M580778); three of us (A.O.G., X.-T.K. and L.K.K.) were supported by the Volkswagen Foundation (Germany). In addition, A.O.G. acknowledges support via the Chang Jiang (Yangtze River) Chair Professorship (China).

REFERENCES

(1) Albert Guijarro, M. Y. *The Origin of Chirality in the Molecules of Life: A Revision from Awareness to the Current Theories and Perspectives of This Unsolved Problem;* ROYAL SOCIETY OF CHEMISTRY, 2008.

(2) Fasman, G. D., Ed. *Circular Dichroism and the Conformational Analysis of Biomolecules;* Springer US, 1996.

(3) Fan, Z.; Govorov, A. O. *Nano Lett.* **2010,** *10*, 2580-2587.

(4) Kuzyk, A.; Schreiber, R.; Fan, Z.; Pardatscher, G.; Roller, E.-M.; Högele, A.; Simmel, F. C.; Govorov, A. O.; Liedl, T. *Nature* **2012,** *483*, 311-314.

(5) Kuzyk, A.; Schreiber, R.; Zhang, H.; Govorov, A. O.; Liedl, T.; Liu, N. *Nat. Mater.* **2014,** *13*, 862-866.

(6) Fan, Z.; Govorov, A. O. *Nano Lett.* **2012,** *12*, 3283-3289.

(7) Mark, A. G.; Gibbs, J. G.; Lee, T.-C.; Fischer, P. *Nat. Mater.* **2013,** *12*, 802-807.

(8) Liu, S.; Han, L.; Duan, Y.; Asahina, S.; Terasaki, O.; Cao, Y.; Liu, B.; Ma, L.; Zhang, J.; Che, S. *Nat. Commun.* **2012,** *3*, 1215.

(9) Ben-Moshe, A.; Wolf, S. G.; Sadan, M. B.; Houben, L.; Fan, Z.; Govorov, A. O.; Markovich, G. *Nat. Commun.* **2014,** *5*, 4302.

(10) Wang, P.-P.; Yu, S.-J.; Govorov, A. O.; Ouyang, M. *Nat. Commun.* **2017,** *8*, 14312.

(11) Mukhina, M. V.; Korsakov, I. V.; Maslov, V. G.; Purcell-Milton, F.; Govan, J.; Baranov, A. V.; Fedorov, A. V.; Gun'ko, Y. K. *Sci. Rep.* **2016,** *6*, 24177.

(12) Govorov, A. O.; Fan, Z.; Hernandez, P.; Slocik, J. M.; Naik, R. R. *Nano Lett.* **2010,** *10*, 1374-1382.

(13) Slocik, J. M.; Govorov, A. O.; Naik, R. R. *Nano Lett.* **2011,** *11*, 701-705.

(14) Govorov, A. O.; Gun; Slocik, J. M.; G; Fan, Z.; Naik, R. R. *J. Mater. Chem.* **2011,** *21*, 16806.

(15) Maoz, B. M.; Chaikin, Y.; Tesler, A. B.; Elli, O. B.; Fan, Z.; Govorov, A. O.; Markovich, G. *Nano Lett.* **2013,** *13*, 1203-1209.

(16) Ben-Moshe, A.; Maoz, B. M.; Govorov, A. O.; Markovich, G. *Chem. Soc. Rev.* **2013,** *42*, 7028.

(17) Shen, X.; Zhan, P.; Kuzyk, A.; Liu, Q.; Asenjo-Garcia, A.; Zhang, H.; Abajo, F. J. G.; Govorov, A.; Ding, B.; Liu, N. *Nanoscale* **2014,** *6*, 2077.

(18) Kuwata-Gonokami, M.; Saito, N.; Ino, Y.; Kauranen, M.; Jefimovs, K.; Vallius, T.; Turunen, J.; Svirko, Y. *Phys. Rev. Lett.* **2005,** *95*, 227401.

(19) Fedotov, V. A.; Schwanecke, A. S.; Zheludev, N. I.; Khardikov, V. V.; Prosvirnin, S. L. *Nano Lett.* **2007,** *7*, 1996-1999.

(20) Hendry, E.; Carpy, T.; Johnston, J.; Popland, M.; Mikhaylovskiy, R. V.; Lapthorn, A. J.; Kelly, S. M.; Barron, L. D.; Gadegaard, N.; Kadodwala, M. *Nat. Nanotechnol.* **2010,** *5*, 783-787.

(21) Collins, J. T.; Kuppe, C.; Hooper, D. C.; Sibilia, C.; Centini, M.; Valev, V. K. *Adv. Opt. Mater.* **2017,** *5*, 1700182.

(22) Ye, W.; Yuan, X.; Guo, C.; Zhang, J.; Yang, B.; Zhang, S. *Phys. Rev. Appl.* **2017,** *7*, 054003.

(23) Hentschel, M.; Schäferling, M.; Weiss, T.; Liu, N.; Giessen, H. *Nano Lett.* **2012,** *12*, 2542-2547.

(24) Li, W.; Coppens, Z. J.; Besteiro, L. V.; Wang, W.; Govorov, A. O.; Valentine, J. *Nat. Commun.* **2015,** *6*, 8379.

(25) Zhao, Y.; Saleh, A. A. E.; Haar, M. A.; Baum, B.; Briggs, J. A.; Lay, A.; Reyes-Becerra, O. A.; Dionne, J. A. *Nat. Nanotechnol.* **2017,** *12*, 1055-1059.

(26) Jain, P. K.; El-Sayed, I. H.; El-Sayed, M. A. *Nano Today* **2007,** *2*, 18-29.

(27) Govorov, A. O.; Richardson, H. H. *Nano Today* **2007,** *2*, 30-38.

(28) Cognet, L.; Tardin, C.; Boyer, D.; Choquet, D.; Tamarat, P.; Lounis, B. *Proc. Natl. Acad. Sci. U.S.A.* **2003,** *100*, 11350-11355.

(29) Gobin, A. M.; O; Watkins, D. M.; Halas, N. J.; Drezek, R. A.; West, J. L. *Lasers Surg. Med.* **2005,** *37*, 123-129.

(30) Skirtach, A. G.; Dejugnat, C.; Braun, D.; Susha, A. S.; Rogach, A. L.; Parak, W. J.; Möhwald, H.; Sukhorukov, G. B. *Nano Lett.* **2005,** *5*, 1371-1377.

(31) Li, M.; Lohmüller, T.; Feldmann, J. *Nano Lett.* **2014,** *15*, 770-775.

(32) Assanov, G. S.; Zhanabaev, Z. Z.; Govorov, A. O.; Neiman, A. B. *Eur. Phys. J.: Spec. Top.* **2013,** *222*, 2697-2704.

(33) Vetrone, F.; Naccache, R.; Zamarrón, A.; Fuente, A. J.; Sanz-Rodríguez, F.; Maestro, L. M.; Rodriguez, E. M.; Jaque, D.; Solé, J. G.; Capobianco, J. A. *ACS Nano* **2010,** *4*, 3254-3258.

(34) Qiu, J.; Wei, W. D. *J. Phys. Chem. C* **2014,** *118*, 20735-20749.

(35) Richardson, H. H.; Hickman, Z. N.; Govorov, A. O.; Thomas, A. C.; Zhang, W.; Kordesch, M. E. *Nano Lett.* **2006,** *6*, 783-788.

(36) Richardson, H. H.; Carlson, M. T.; Tandler, P. J.; Hernandez, P.; Govorov, A. O. *Nano Lett.* **2009,** *9*, 1139-1146.

(37) Rohani, S.; Quintanilla, M.; Tuccio, S.; Angelis, F. D.; Cantelar, E.; Govorov, A. O.; Razzari, L.; Vetrone, F. *Adv. Opt. Mater.* **2015,** *3*, 1606-1613.

(38) Govorov, A. O.; Zhang, W.; Skeini, T.; Richardson, H.; Lee, J.; Kotov, N. A. *Nanoscale Res. Lett.* **2006,** *1*, 84-90.

(39) Govorov, A. O.; Fan, Z.; Neiman, A. B. Photothermal Effect of Plasmonic Nanoparticles and Related Bioapplications. In *Complex-Shaped Metal Nanoparticles;* Sau, T. K., Rogach, A. L., Eds.; Wiley-VCH Verlag GmbH & Co. KGaA, 2012; pp 455-475.

(40) Keblinski, P.; Cahill, D. G.; Bodapati, A.; Sullivan, C. R.; Taton, T. A. *J. Appl. Phys.* **2006,** *100*, 054305.

(41) Maier, S. A. *Plasmonics: Fundamentals and Applications;* Springer US, 2007.

(42) Watts, C. M.; Liu, X.; Padilla, W. J. *Adv. Mater.* **2012,** *24*, OP98--OP120.

(43) Landy, N. I.; Sajuyigbe, S.; Mock, J. J.; Smith, D. R.; Padilla, W. J. *Phys. Rev. Lett.* **2008,** *100*, 207402.

(44) Liu, X.; Tyler, T.; Starr, T.; Starr, A. F.; Jokerst, N. M.; Padilla, W. J. *Phys. Rev. Lett.* **2011,** *107*, 045901.

(45) Maier, T.; Brueckl, H. *Opt. Lett.* **2010,** *35*, 3766.

(46) Yu, P.; Wu, J.; Ashalley, E.; Govorov, A.; Wang, Z. *J. Phys. D: Appl. Phys.* **2016,** *49*, 365101.

(47) Carslaw, H. S.; Jaeger, J. C. *Conduction of Heat in Solids;* OXFORD UNIV PR, 1993.

(48) Jack, C.; Karimullah, A. S.; Tullius, R.; Khorashad, L. K.; Rodier, M.; Fitzpatrick, B.; Barron, L. D.; Gadegaard, N.; Lapthorn, A. J.; Rotello, V. M.; Cooke, G.; Govorov, A. O.; Kadodwala, M. *Nat. Commun.* **2016,** *7*, 10946.

(49) Sykes, M. E.; Stewart, J. W.; Akselrod, G. M.; Kong, X.-T.; Wang, Z.; Gosztola, D. J.; Martinson, A. B. F.; Rosenmann, D.; Mikkelsen, M. H.; Govorov, A. O.; Wiederrecht, G. P. *Nat. Commun.* **2017,** *8*, 986.

(50) Johnson, P. B.; Christy, R. W. *Phys. Rev. B* **1972,** *6*, 4370-4379.

(51) Fan, Z.; Zhang, H.; Govorov, A. O. *J. Phys. Chem. C* **2013,** *117*, 14770-14777.

(52) Khorashad, L. K.; Besteiro, L. V.; Wang, Z.; Valentine, J.; Govorov, A. O. *J. Phys. Chem. C* **2016,** *120*, 13215-13226.

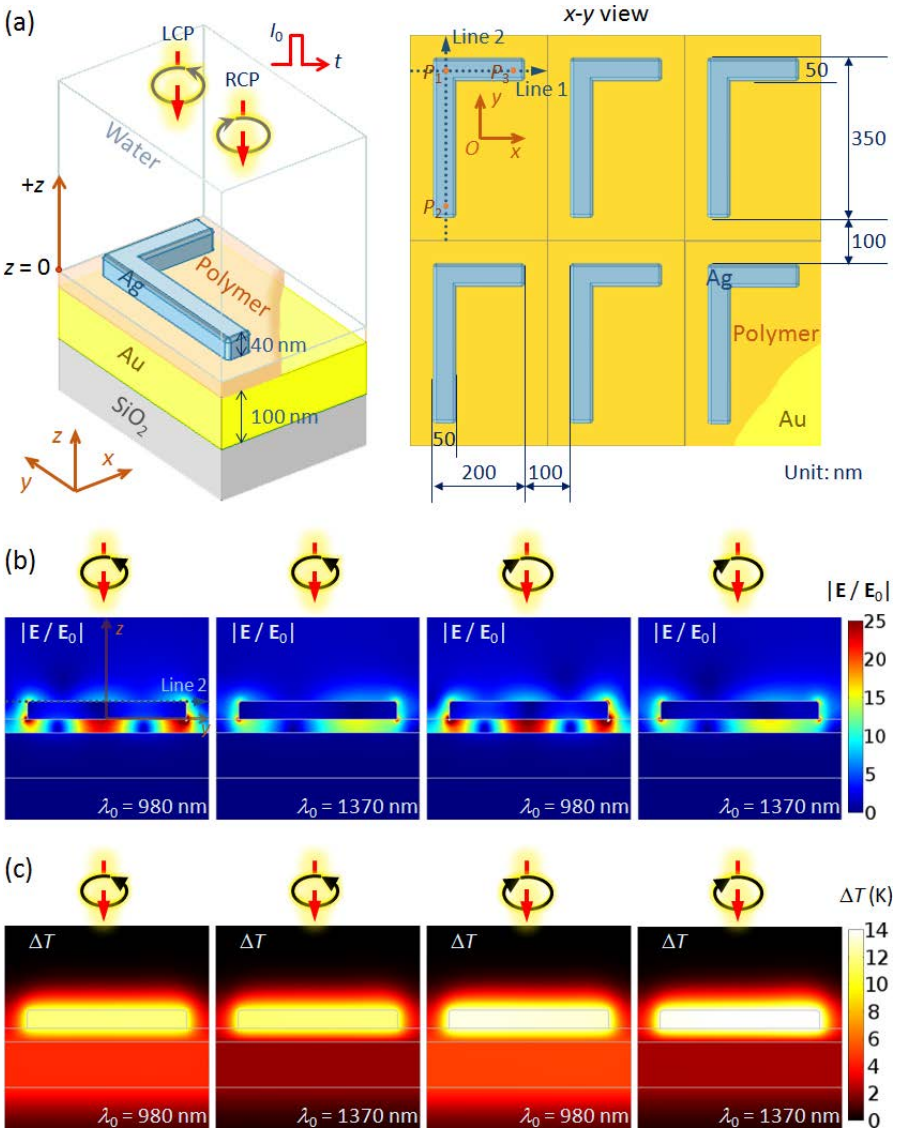

Figure 1. (a) Geometry of the chiral absorber with the coordinate system and definitions of incident circularly polarized beams. The top surface of the Γ-nanostructure is rounded by a radius of 7 nm. (b) Spatial maps of the electromagnetic field inside the metastructure at the two plasmonic wavelengths for the vertical cross section coming through Line 2 shown in (a); the system is under CW excitation. We see that the system is strongly chiral since the patterns for LCP and RCP beams are very different. (c) The photothermal maps of the chiral absorber. The data are given at the time t = 8 ns for the incident light flux of $I_0 = 10^5$ W/cm^2. We see now a strong difference in the magnitude of photoinduced temperature for the LCP and RCP beams. Since the optical CD signals are negative in our structure, the phototemperature for RCP light is higher. In (b, c), the polymer spacer thickness is 30 nm.

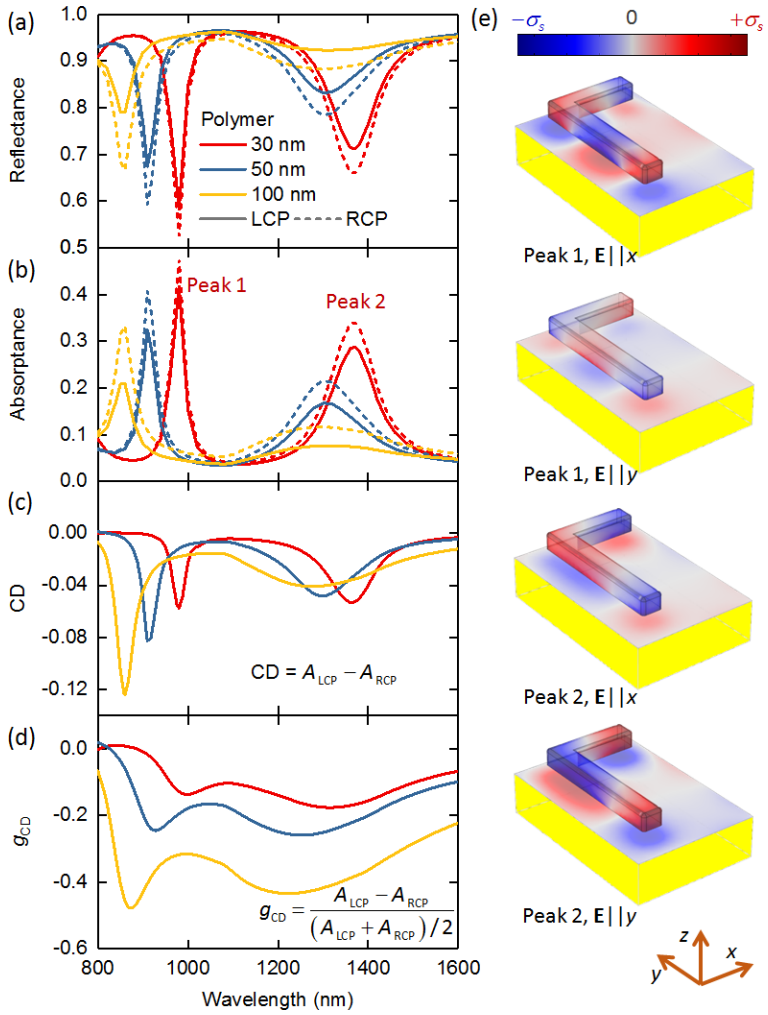

Figure 2. Optical and chiro-optical properties of the metastructure absorber. The graphs show the spectra of reflection (a), absorption (b), CD (c) and g_{CD} factor (d) of the metastructures with three different polymer thicknesses ($t_{polymer}$ = 30, 50, 100 nm). In (a, b), solid and dashed lines show the spectra with incidence of LCP and RCP beams, respectively. (e) Surface change distributions for the two main plasmonic modes with the linear polarizations. We see from the amplitudes of surface charges that the plasmonic absorption at Peak 1 comes mostly from the excitation with **E**||*x*; whereas the long-wavelength plasmonic absorption at Peak 2 is associated mainly with the polarization of **E**||*y*. In (e), the polymer thickness is 30 nm.

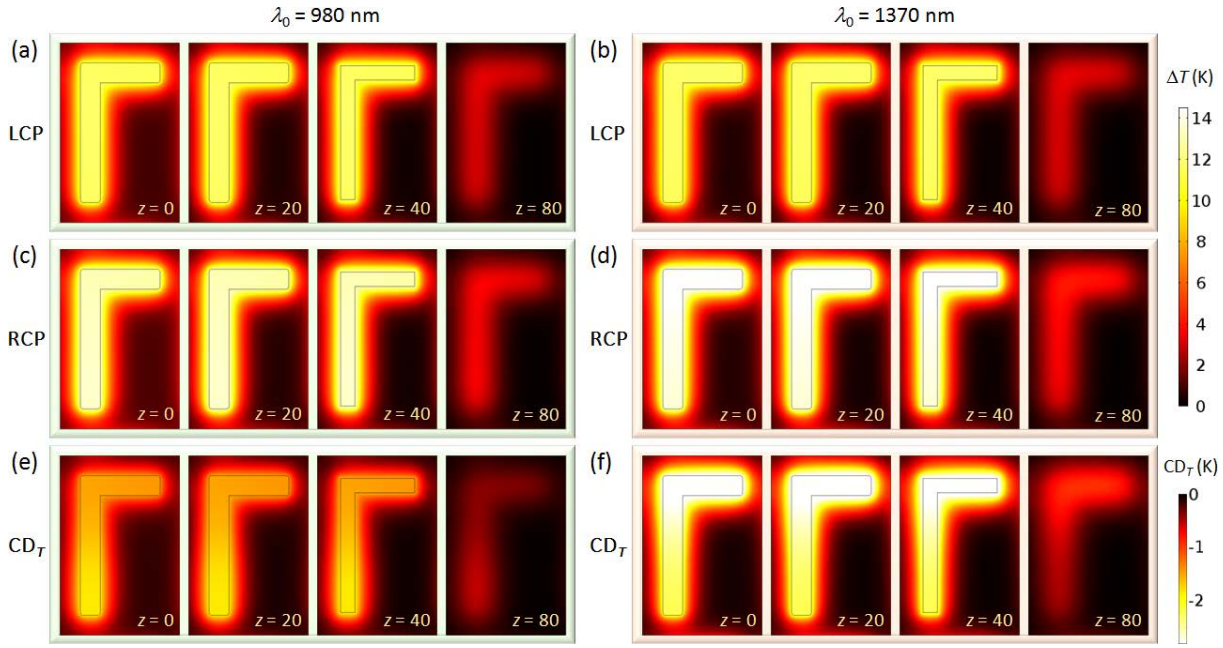

Figure 3. Photoinduced temperature increase, ΔT, with LCP (a, b) and RCP (c, d) incident beams and photothermal CD distributions (e, f) at the two plasmonic resonance wavelengths in the horizontal cross sections (z = 0, 20, 40, 80 nm). The polymer thickness is t_{polymer} = 30 nm. The incident light flux is $I_0 = 10^5$ W/cm^2. The data are given at the time of t = 8 ns. The free space wavelength of the incident light is λ_0 = 980 nm in (a, c, e) and λ_0 = 1370 nm in (b, d, f).

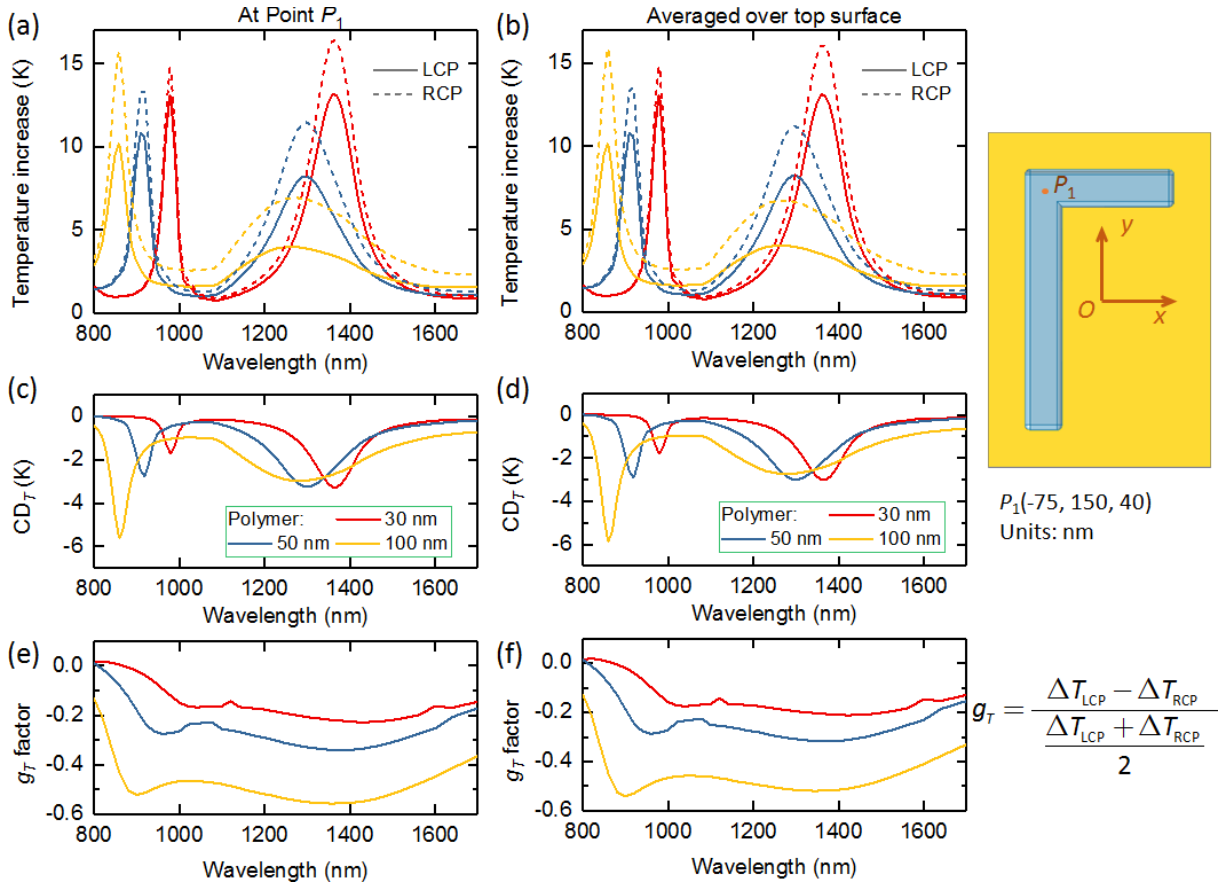

Figure 4. The position-dependent photothermal and photoinduced chiro-thermal properties of the metastructures with three different polymer thicknesses ($t_{polymer}$ = 30, 50, 100 nm). The incident light flux is $I_0 = 10^5$ W/cm^2. The data are given at the time of t = 8 ns. (a, b) Spectra of temperature increase, $\Delta T(\lambda_0)$. The solid and dashed lines show the spectra with the incidence of LCP and RCP beams, respectively. (c, d) Photothermal CD spectra, $CD_T(\lambda_0)$. (e, f) Spectra of the thermal g-factor, $g_T(\lambda_0)$. In (a, c, e), these local properties are given for a specific position, Point P_1. In (b, d, f), the data are averaged over the top surface of the Γ-structure.

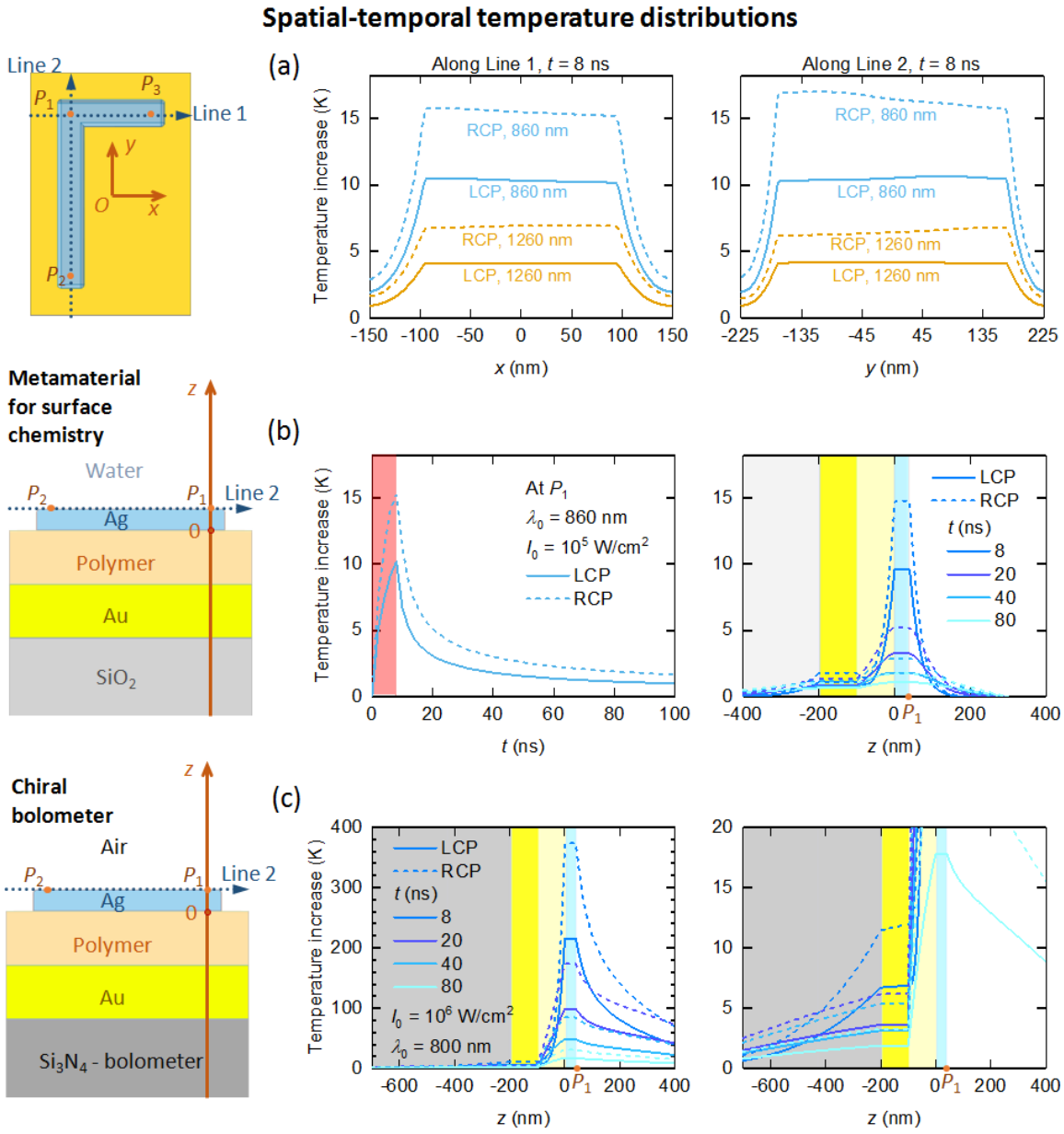

Figure 5. Spatial-temporal temperature distributions in the chiral metastructures. (a, b) The temperature distributions of the metastructure with polymer thickness of $t_{polymer}$ = 100 nm for excitation of LCP and RCP beams with the incident flux $I_0 = 10^5$ W/cm^2. (a) Horizontal spatial temperature distributions at time t = 8 ns at the two plasmonic resonance wavelengths of λ_0 = 860 and 1260 nm along Line 1 (left) and Line 2 (right). (b) Temporal and vertical spatial temperature distributions at the first plasmonic resonance wavelength (λ_0 = 860 nm). Left: over time, the temperature exponentially accumulates during the optical pulse excitation and exponentially decreases after the pulse. The pulse duration is highlighted with red background. The data are given at Point P_1 on the top surface of the Γ-shape. Right: temperature distribution after the pulse excitation at t = 8, 20, 40, 80 ns along the vertical line across P_1. (c) The spatial temperature

distribution in the chiral bolometer consisting of Air/Ag Γ-nanostructure/100nm-polymer/Au slab/Si_3N_4 substrate at t = 8, 20, 40, 80 ns along the vertical line across P_1. The data are given at the first plasmonic resonance wavelength, which shifts to λ_0 = 800 nm. The incident light flux is $I_0 = 10^6$ W/cm^2. Right: zoomed-in region showing the propagation of heat into the bolometric substrate.